

Strong-Coupling Superconductivity with $T_c \sim 10.8$ K Induced by P doping in the Topological Semimetal Mo_5Si_3

Bin-Bin Ruan^{1*†}, Jun-Nan Sun^{1,2,3†}, Yin Chen^{1,4}, Qing-Song Yang^{1,5}, Kang Zhao^{1,6}, Meng-Hu Zhou¹, Ya-Dong Gu^{1,5}, Ming-Wei Ma^{1,7}, Gen-Fu Chen^{1,5,7}, Lei Shan^{2,3*} and Zhi-An Ren^{1,5*}

¹ Institute of Physics and Beijing National Laboratory for Condensed Matter Physics, Chinese Academy of Sciences, Beijing 100190, China

² Information Materials and Intelligent Sensing Laboratory of Anhui Province, Institutes of Physical Science and Information Technology, Anhui University, Hefei 230601, China

³ Key Laboratory of Structure and Functional Regulation of Hybrid Materials (Anhui University), Ministry of Education, Hefei 230601, China

⁴ School of Materials Science and Engineering, University of Science and Technology Beijing, Beijing 100083, China

⁵ School of Physical Sciences, University of Chinese Academy of Sciences, Beijing 100049, China

⁶ Pilot National Laboratory for Marine Science and Technology, Qingdao, Shandong 266237, China

⁷ Songshan Lake Materials Laboratory, Dongguan, Guangdong 523808, China

ABSTRACT

By performing P doping on the Si sites in the topological semimetal Mo_5Si_3 , we discover strong-coupling superconductivity in $\text{Mo}_5\text{Si}_{3-x}\text{P}_x$ ($0.5 \leq x \leq 2.0$). Mo_5Si_3 crystallizes in the $W_5\text{Si}_3$ -type structure with space group of $I4/mcm$ (No. 140), and is not a superconductor itself. Upon P doping, the lattice parameter a decreases while c increases monotonously. Bulk superconductivity is revealed in $\text{Mo}_5\text{Si}_{3-x}\text{P}_x$ ($0.5 \leq x \leq 2.0$) from resistivity, magnetization, and heat capacity measurements. T_c in $\text{Mo}_5\text{Si}_{1.5}\text{P}_{1.5}$ reaches as high as 10.8 K, setting a new record among the $W_5\text{Si}_3$ -type superconductors. The upper and lower critical fields for $\text{Mo}_5\text{Si}_{1.5}\text{P}_{1.5}$ are 14.56 T and 105 mT, respectively. Moreover, $\text{Mo}_5\text{Si}_{1.5}\text{P}_{1.5}$ is found to be a fully gapped superconductor with strong electron-phonon coupling. First-principles calculations suggest that the enhancement of electron-phonon coupling is possibly due to the shift of the Fermi level, which is induced by electron doping. The calculations also reveal the nontrivial band topology in Mo_5Si_3 . The T_c and upper critical field in $\text{Mo}_5\text{Si}_{3-x}\text{P}_x$ are fairly high among pseudobinary compounds. Both of them are higher than those in NbTi, making future applications promising. Our results suggest that the $W_5\text{Si}_3$ -type compounds are ideal platforms to search for new superconductors. By examinations of their band topologies, more candidates for topological superconductors can be expected in this structural family.

Keywords: Mo_5Si_3 , superconductivity, doping, topological insulator, electron-phonon coupling

* Corresponding authors (email: bbuan@mail.ustc.edu.cn; lshan@ahu.edu.cn; renzhian@iphy.ac.cn)

† These authors contributed equally to this work.

INTRODUCTION

Topological superconductors, hosting both gapped bulk superconducting states and gapless surface states, have attracted much attention in recent years. The most fascinating feature in a topological superconductor is that its quasiparticle excitations form Majorana zero modes (MZMs) at boundaries and vortices [1-3]. The MZMs obey the non-Abelian statistics, and are thus suitable for the realization of fault-tolerant quantum computations [4, 5].

In view of the above intriguing merits, much effort has been devoted to seek for topological superconductivity in real materials. One approach is to search for superconductors with odd parity, as demonstrated in Sr_2RuO_4 , $\text{Sn}_{1-x}\text{In}_x\text{Te}$, or $T_d\text{-MoTe}_2$ [6-9]. However, odd-parity superconductors are very rare, and their superconductivity is generally fragile to impurities or disorders. Moreover, all these superconductors have very low (< 2 K) superconducting transition temperatures (T_c s), limiting possible applications. Another approach, as proposed by Fu and Kane [10], is to fabricate heterostructures made of superconductors and topological insulators, where the topological surface states (TSSs) become superconducting from the proximity effect. The realizations [11-13], however, require delicate device fabrications and face the challenges of lattice mismatch and interface complexity.

Consequently, researchers in this field have been moving much of their attention to find bulk superconductors that also possess nontrivial band topologies. Such conception is simple but effective. In this spirit, superconducting topological materials such as $\beta\text{-PdBi}_2$, doped Bi_2Se_3 , PdBi , 2M-WS_2 were proposed to be candidates for topological superconductors [14-21]. In many of them, spectroscopy methods such as scanning tunneling microscopy (STM) and angle-resolved photoemission spectroscopy (ARPES) successfully confirmed the existence of TSSs [20-23], which in turn verified the effectiveness of the conception.

Recently, superconductivity was observed in Re doped Mo_5Si_3 , with a maximal T_c of 5.8 K in $\text{Mo}_3\text{Re}_2\text{Si}_3$ [24]. Not only did Ref. 24 set a record-high T_c in W_5Si_3 -type superconductors, it also emphasized the nontrivial band topology, making $\text{Mo}_3\text{Re}_2\text{Si}_3$ a candidate for topological superconductors. We noticed that, just like the cases of Cu/Sr/Nb doped Bi_2Se_3 [14-17, 19], superconductivity was successfully induced by carrier doping in topological material Mo_5Si_3 . We thus systematically examined the doping effects not only on the Mo sites, but also on the Si sites in Mo_5Si_3 .

In this paper, we report detailed characterizations of $\text{Mo}_5\text{Si}_{3-x}\text{P}_x$ ($0 \leq x \leq 2.0$), in which bulk superconductivity with T_c as high as 10.8 K is observed. In addition, $\text{Mo}_5\text{Si}_2\text{P}$ and $\text{Mo}_5\text{Si}_{1.5}\text{P}_{1.5}$ are found to host strong electron-phonon coupling. The enhancement of the coupling strength is due to the shift of the Fermi level, and possibly the phonon softening, as revealed by the heat capacity measurements and first-principles calculations. A series of superconducting parameters for $\text{Mo}_5\text{Si}_{1.5}\text{P}_{1.5}$ are determined, and the electronic band topologies are briefly discussed.

METHODS

Polycrystalline samples of $\text{Mo}_5\text{Si}_{3-x}\text{P}_x$ ($x = 0, 0.5, 1.0, 1.2, 1.3, 1.5, 1.6, \text{ and } 2.0$) were prepared by solid state reaction. Elements of Mo (99.9%, powder), Si (99.999%, powder), and P (99.99%, powder) were mixed thoroughly before pressed into pellets. The pellets were placed into alumina crucibles before sealed into silica tubes under argon. The tubes were slowly heated to 1073 K and held for 24 hours. Then the products were thoroughly ground, pressed into pellets, put into alumina crucibles, and sealed into tantalum tubes under argon. The tubes were heated under high-purity argon at 1923 K for 20 hours. All the manipulations except sealing and heating were carried out in a glove box filled with high-purity argon. The final products showed silver metallic lusters and were stable in air.

The room temperature powder x-ray diffraction (XRD) data were collected on a PAN-analytical x-ray diffractometer with $\text{Cu-K}\alpha$ radiation. Rietveld refinements were carried out using the GSAS package [25]. The resistivity and heat capacity data were collected on a physical property measurement system (PPMS, Quantum Design). The magnetization measurements were performed on a magnetic property measurement system (MPMS, Quantum Design). The chemical compositions were determined by an energy-dispersive x-ray (EDX) spectrometer

equipped on a Phenom ProX scanning electron microscope. More details about the measurements can be found in our previous study [26].

First-principles calculations were performed based on the density functional theory (DFT), as implemented in the QUANTUM ESPRESSO package [27]. The exchange-correlation functionals of PBE based on the generalized gradient approximation (GGA) were chosen. The optimized normconserving pseudopotentials [28] were used. Before the calculations for charge densities, the lattice parameters, as well as the atomic positions, were fully relaxed until the force on each atom was less than 0.0001 Ry/Bohr. A Monkhorst–Pack grid of $15 \times 15 \times 11$ was applied in the self-consistent calculations. P doping on the Si sites was treated by the method of virtual crystal approximation (VCA). The validation of VCA has been checked with the supercell results. (see Supplementary Information)

RESULTS

Structural characterizations

Figure 1(a) demonstrates the crystal structure of $\text{Mo}_5\text{Si}_{3-x}\text{P}_x$, one may notice that the structure features Si–Si chains along the c axis. XRD patterns of polycrystalline $\text{Mo}_5\text{Si}_{3-x}\text{P}_x$ ($0 \leq x \leq 2.0$) are shown in Figure 1(e). Without P doping, a phase pure Mo_5Si_3 sample, which is of the tetragonal W_5Si_3 type (space group $I4/mcm$), is successfully obtained. Upon doping, an impurity phase of Mo_3P emerges. Using MoP precursor instead of P in the preparation procedure was found to be beneficial to reduce the amount of Mo_3P in the final products. However, we were not able to completely remove the Mo_3P impurity. This is possibly due to the inevitable evaporation of P at high temperature. As a result, the actual contents of P in the products should be less than the nominal ones, which was confirmed by our EDX measurements. The measured values of x are listed in Table 1, and are plotted in Figure 1(d). Notice that the measured P contents are not far from the nominal ones. For simplification, x in $\text{Mo}_5\text{Si}_{3-x}\text{P}_x$ mentioned hereafter represent the nominal values.

The diffraction peaks of $\text{Mo}_5\text{Si}_{3-x}\text{P}_x$ evidently shift with x increasing, as shown in Figure 1(f). To gain insights into the crystallographic parameters, we performed Rietveld refinements to each XRD pattern. Details of the refinement results are listed in Table 1. Two of them ($x = 0.5$ and $x = 1.5$) are shown as examples in Figure 1(b). The small values of R_p , R_{wp} , and χ^2 suggest the refinements are satisfactory. As shown in Figure 1(c), the a -axis shrinks while the c -axis expands monotonously, indicating a successful P doping into Mo_5Si_3 . This doping behavior is different from that in $\text{Mo}_{5-x}\text{Re}_x\text{Si}_3$, where only the a -axis was changed [24]. We note that the shrinkage of a -axis of Mo_5SiP_2 compared with Mo_5Si_3 is around 1.6%, while the changes of the lattice parameters of Mo_3P impurity are less than 0.1%. This means that the Si doping content in Mo_3P is insignificant (if not zero) in our samples. There are two different Wyckoff positions (Si1 at $4a$ and Si2 at $8h$) of Si in Mo_5Si_3 . Therefore, there could be a site-selection in P doping. We carefully examined the evolution of all the bond lengths in $\text{Mo}_5\text{Si}_{3-x}\text{P}_x$. However, no evidence backing this assumption was found. No reflections from supercell were observed in the XRD patterns either. P is thus believed to randomly take all the Si sites. (We should note that it is generally very difficult to distinguish P from Si by XRD measurements, so chances are that there still exists nonequivalent doping between the Si1 and Si2 sites.) The shrinkage of a and expansion of c are consistent with our DFT relaxation results. (see Supplementary Information)

Superconducting properties

The temperature dependence of electrical resistivity (ρ) for $\text{Mo}_5\text{Si}_{3-x}\text{P}_x$ ($0 \leq x \leq 2.0$) is shown in Figure 2(a). All of the samples show metallic behaviors. For the undoped sample Mo_5Si_3 , ρ reads ~ 0.22 m Ω cm at 300 K and decreases monotonously with the decrease of temperature. $\rho(T)$ for Mo_5Si_3 shows no superconducting transitions down to 1.8 K. These results are in good agreement with those in the references [24, 29], where no superconductivity was observed above 0.15 K. P doping into Mo_5Si_3 introduces superconductivity, as revealed by abrupt drops of $\rho(T)$ curves for the doped samples. The region of the superconducting transitions is emphasized in Figure 2(b). For the samples

with $x \geq 1.0$, the normal state $\rho(T)$ curves obviously show upwards concave features, similar to those observed in the A15 compounds, which can be interpreted by a parallel-resistor model [30].

To investigate the magnetic properties of the superconducting samples, the DC magnetic susceptibility ($4\pi\chi$) of $\text{Mo}_5\text{Si}_{3-x}\text{P}_x$ ($0.5 \leq x \leq 2.0$) was measured and is shown in Figure 2(c). Notice the data have been corrected with the corresponding demagnetization factors. In the zero-field-cooling (ZFC) run, $4\pi\chi$ of each sample quickly approaches a constant at low temperature, indicating the occurrence of superconductivity. The shielding fractions are close to or larger than 100%, validating bulk superconductivity in $\text{Mo}_5\text{Si}_{3-x}\text{P}_x$. T_c s can be determined from the onset temperature to deviate from the normal states, which are in good agreements with those obtained from the $\rho(T)$ data. It should be mentioned that the diamagnetic signals of Mo_3P ($T_c = 5.6$ K [31]) in the $4\pi\chi(T)$ curves are negligible (it is obvious only in the heavily doped sample Mo_5SiP_2). This is presumably due to the shielding effects of $\text{Mo}_5\text{Si}_{3-x}\text{P}_x$, which have higher T_c s than Mo_3P . The absolute values of $4\pi\chi$ in the field-cooling (FC) runs are significantly lower than those in the ZFC runs, indicating large pinning effects in the superconducting samples.

Gathering the data from $\rho(T)$ and $4\pi\chi(T)$, we are able to conclude the evolution of T_c in $\text{Mo}_5\text{Si}_{3-x}\text{P}_x$ ($0 \leq x \leq 2.0$), as listed in Table 1, and shown in Figure 2(d). Non-superconducting Mo_5Si_3 becomes superconducting with P doping. T_c quickly increases, exceeding 10 K in $\text{Mo}_5\text{Si}_{1.8}\text{P}_{1.2}$, while further P doping brings up little change in T_c . Simultaneously, the residual resistivity ratio (RRR) decreases regularly upon P doping, which is reasonable since P doping introduces more defects in the sample.

Now we move on to the discussion of the superconducting nature by conducting a detailed investigation on the $\text{Mo}_5\text{Si}_{1.5}\text{P}_{1.5}$ sample. We choose to characterize this sample in detail because it hosts the highest T_c , and has less Mo_3P impurities compared with heavier-doped samples. $\rho(T)$ of $\text{Mo}_5\text{Si}_{1.5}\text{P}_{1.5}$ under various magnetic fields ($\mu_0H = 0 - 15.5$ T) is shown in Figure 3(a). Under zero magnetic field, $\rho(T)$ starts to drop abruptly at a T_c^{onset} of 10.80 K, and reaches zero at a T_c^{zero} of 10.70 K, resulting in a superconducting transition width of only 0.1 K. Upon the application of magnetic field, superconductivity in $\text{Mo}_5\text{Si}_{1.5}\text{P}_{1.5}$ is gradually suppressed. T_c under different magnetic fields is determined by the 50% criterion, *i.e.* the temperature where $\rho(T)$ reaches 50% of that of the normal state. The phase diagram of upper critical field (μ_0H_{c2}) versus T is therefore plotted in Figure 3(d). It can be seen that the Ginzburg–Landau (G–L) model $\mu_0H_{c2}(T) = \mu_0H_{c2}(0)[1 - (T/T_c)^2] / [1 + (T/T_c)^2]$ gives a satisfying fit of the experimental results in the whole temperature range. $\mu_0H_{c2}(0)$ is fitted to be 14.56 T, which is lower than the Pauli paramagnetic limit (20.0 T).

We have also performed isothermal magnetization measurements on $\text{Mo}_5\text{Si}_{1.5}\text{P}_{1.5}$. The hysteresis loop at 2 K is shown in Figure 3(c). A typical behavior of a type-II superconductor is observed. The isothermal magnetization curves under various temperatures are shown in Figure 3(b), from which the lower critical field (μ_0H_{c1}) can be determined from the deviation of the curves from the initial Meissner states. μ_0H_{c1} under different temperature is plotted in Figure 3(d). One can easily fit $\mu_0H_{c1}(T)$ with the well-known G–L expression: $\mu_0H_{c1}(T) = \mu_0H_{c1}(0)(1 - t^2)$, where t is the normalized temperature T/T_c . The fit gives a $\mu_0H_{c1}(0)$ of 105 mT.

Based on the results of $\mu_0H_{c1}(0)$ and $\mu_0H_{c2}(0)$, a series of superconducting parameters can be obtained. The G–L coherence length (ξ_{GL}) of $\text{Mo}_5\text{Si}_{1.5}\text{P}_{1.5}$ is calculated to be 4.75 nm by the relation: $\mu_0H_{c2}(0) = \Phi_0 / (2\pi\xi_{\text{GL}}^2)$, in which Φ_0 stands for the magnetic flux quantum. The superconducting penetration depth (λ_{GL}) is calculated by $\mu_0H_{c1}(0) = \Phi_0 / (4\pi\lambda_{\text{GL}}^2)(\ln\kappa + 0.5)$, where $\kappa \equiv \lambda_{\text{GL}} / \xi_{\text{GL}}$ is the G–L parameter. Consequently, we obtain $\lambda_{\text{GL}} = 70.5$ nm and $\kappa = 14.8$. The value of κ is far larger than $1/\sqrt{2}$, again suggesting $\text{Mo}_5\text{Si}_{1.5}\text{P}_{1.5}$ to be a type-II superconductor. The thermodynamic critical field can therefore be determined by $\mu_0H_c(0) = \mu_0\sqrt{H_{c1}(0)H_{c2}(0) / \ln\kappa}$ to be 0.75 T. All these superconducting parameters are summarized in Table 2.

In order to take more insight into the superconductivity, as well as the thermodynamic properties of $\text{Mo}_5\text{Si}_{3-x}\text{P}_x$, we measured the specific heat (C_p) of $\text{Mo}_5\text{Si}_{3-x}\text{P}_x$ ($x = 0, 1.0, 1.5$). As the doped samples contained superconducting

Mo₃P, we synthesized a phase pure Mo₃P sample, whose $C_p(T)$ was measured before subtracted from the raw data of Mo₅Si_{3-x}P_x. (see Supplementary Information) This approach is similar to that in Mo₅PB₂ [32]. The corrected data are shown in Figure 4. No superconducting transitions are observed in Mo₅Si₃, while clear anomalies are found at 8.46 K and 10.62 K for $x = 1.0$ and $x = 1.5$, respectively, evidencing the bulk superconductivity. The values of T_c from C_p measurements correspond well with those from the resistivity and the magnetization measurements. For each sample, the behavior of C_p at the normal state up to 18 K can be well described with the Debye model: $C_p(T) = \gamma T + \beta T^3 + \delta T^5$, in which the three terms stand for the Sommerfeld term, the contributions from harmonic phonons and anharmonic phonons, respectively. The fitted curves are shown in Figure 4(a) as the dash lines. γ and β for each sample are listed in Table 2. Notice that from $x = 0$ to $x = 1.5$, γ almost doubles, while β becomes an order of magnitude larger. We calculate the Debye temperature (Θ_D) by $\Theta_D = (12\pi^4 NR / 5\beta)^{1/3}$, in which N is the number of atoms per formula unit (f.u.), and R is the ideal gas constant. The results are also listed in Table 2. One may see that P doping greatly reduces the value of Θ_D (from 619 K to 314 K), implying substantial softening of the lattice. This is quite surprising since the atomic mass of P is close to that of Si. The softening of phonons in P doped samples may be related to the emergence of phonon soft modes. Detailed theoretical calculations will help to elucidate this topic in the future.

The electronic contribution to C_p can thus be obtained by subtracting the phonon terms. Temperature dependence of electronic specific heat (C_e) is shown in Figure 4(b). Notice that the normalized C_e jumps at T_c ($\Delta C_e / \gamma T_c$) are 2.03 and 2.06 for Mo₅Si₂P and Mo₅Si_{1.5}P_{1.5}, respectively. These values are much larger than the BCS weak coupling ratio (1.43), suggesting strong coupling in these samples.

For a strong-coupling superconductor, the electron-phonon coupling parameter (λ_{ep}) can be estimated by the McMillan formula modified by Allen and Dynes [33, 34]:

$$T_c = \frac{\omega_{ln}}{1.2} \exp \left[\frac{1.04(1 + \lambda_{ep})}{\mu^* (1 + 0.62\lambda_{ep}) - \lambda_{ep}} \right], \quad (1)$$

where the logarithmic average phonon frequency ω_{ln} is given by [35]:

$$\frac{\Delta C_e}{\gamma T_c} = 1.43 \left[1 + 53 \left(\frac{T_c}{\omega_{ln}} \right)^2 \ln \left(\frac{\omega_{ln}}{3T_c} \right) \right]. \quad (2)$$

By setting the Coulomb screening parameter $\mu^* = 0.13$, we get $\lambda_{ep} = 1.12$ and 1.15 for $x = 1.0$ and $x = 1.5$, respectively. We further calculate the density of states at the Fermi level using $N(E_F) = 3\gamma / [\pi^2 k_B^2 (1 + \lambda_{ep})]$, where k_B is the Boltzmann constant. The calculations give $N(E_F) = 4.99$ and $7.30 \text{ eV}^{-1} \text{ f.u.}^{-1}$ for $x = 1.0$ and $x = 1.5$, respectively.

C_e in the superconducting state is treated by calculating the entropy with [36]:

$$S(T) = -\frac{3\gamma}{\pi^3 k_B} \int_0^{2\pi} \int_0^\infty [f \ln f + (1-f) \ln (1-f)] d\epsilon d\varphi, \quad (3)$$

in which $f = 1 / \left[1 + \exp \left(\sqrt{\epsilon^2 + \Delta^2(\varphi, T)} / k_B T \right) \right]$ stands for the Fermi distribution of the quasiparticles. Here, we find that a conventional s -wave gap function reproduces the data well, and the so-called α model is applied. In this model, the angular independent gap function $\Delta(T)$ is expressed as $\Delta(T) = \alpha / \alpha_{BCS} \Delta_{BCS}(T)$ where α_{BCS} is the weak-coupling gap ratio (1.76) [37]. C_e is calculated from $C_e = T \frac{\partial S}{\partial T}$. Fittings to the C_e data are illustrated in Figure 4(b), from which we obtain the superconducting gap values at zero temperature $\Delta_0 = 1.48$ and 1.96 meV for $x = 1.0$ and $x = 1.5$,

respectively. The coupling strength $\Delta_0/k_B T_c$ are thus estimated to be 2.03 and 2.14. Again, these values apparently exceed α_{BCS} , evidencing strong-coupled superconductivity.

First-principles calculations

The results of first-principles calculations for $\text{Mo}_5\text{Si}_{3-x}\text{P}_x$ ($x = 0, 1.0, 1.5$) are summarized in Figure 5, with the electronic band structures of $x = 0$ (with and without spin-orbit coupling), $x = 1.0$, and $x = 1.5$ shown in Figure 5(a)–(d), respectively. For all these samples, there are multiple bands crossing the Fermi level (E_F), consistent with the metallic nature of $\text{Mo}_5\text{Si}_{3-x}\text{P}_x$. By comparing Figure 5(a) and 5(b), we conclude that the spin-orbit coupling (SOC) has negligible effects on the band structures, although it opens finite gaps on several k points. The shapes of the electronic bands for $\text{Mo}_5\text{Si}_2\text{P}$ and $\text{Mo}_5\text{Si}_{1.5}\text{P}_{1.5}$ are basically the same with that of Mo_5Si_3 , which means that the bands can be considered rigid in our case. One major feature of the band structure in Figure 5(a) is the flat band dispersions at around 0.25 eV above E_F (as indicated by the shadowy box), which gradually shift to E_F when x increases. This process is clearly observed when we examine the evolution of the density of states (DOS) upon P doping (shown in Figure 5(g)). E_F of Mo_5Si_3 locates in a dip of DOS, and it shifts to a major peak for $\text{Mo}_5\text{Si}_{1.5}\text{P}_{1.5}$. Theoretical values of DOS at E_F ($N'(E_F)$) are 4.13, 7.24, and 8.04 $\text{eV}^{-1} \text{f.u.}^{-1}$ for $x = 0, 1.0$, and $x = 1.5$, respectively. The trend of $N'(E_F)$ is consistent with the change of the Sommerfeld parameter γ . We notice that $N'(E_F)$ of $\text{Mo}_5\text{Si}_{1.5}\text{P}_{1.5}$ corresponds fairly well with the experimental one, while $N'(E_F)$ of $\text{Mo}_5\text{Si}_2\text{P}$ is much larger compared with $N(E_F)$. This means that λ_{ep} of $\text{Mo}_5\text{Si}_2\text{P}$ is probably overestimated, and equation (3) is not applicable. In fact, if we use the inverted McMillan formula [34]:

$$\lambda_{\text{ep}} = \frac{1.04 + \mu^* \ln(\Theta_D / 1.45T_c)}{(1 - 0.62\mu^*) \ln(\Theta_D / 1.45T_c) - 1.04}, \quad (4)$$

λ_{ep} and $N(E_F)$ for $\text{Mo}_5\text{Si}_2\text{P}$ are estimated to be 0.69, and 6.30 $\text{eV}^{-1} \text{f.u.}^{-1}$, respectively.

We further examine the band topology of Mo_5Si_3 . Since Mo_5Si_3 possesses both time-reversal symmetry and inversion symmetry, the Z_2 topological invariants can be easily calculated by checking the wavefunction parities on the eight time-reversal invariant k points [38]. As illustrated in Figure 5(b), we calculate the Z_2 indexes for several bands near E_F . Notice that not all these Z_2 indexes are well-defined, since there might be no gap between one band and another. Nevertheless, SOC opens finite gaps between bands 160 and 162, and between bands 164 and 166. Z_2 indexes for these two gaps are (0;111) and (0;000), respectively. Our results are consistent with previous studies [24, 39], suggesting that bulk Mo_5Si_3 (with SOC) falls into the weak topological insulator state. Unfortunately, this means that the TSSs in Mo_5Si_3 are fragile, and are unlikely to survive with P doping, which inevitably introduces defects. What makes it worse is that E_F shifts to higher energies in the doped samples, which could push the system into a topologically trivial state. In a word, P doping into Mo_5Si_3 may destroy its TSSs, making it less possible to realize topological superconductivity in $\text{Mo}_5\text{Si}_{3-x}\text{P}_x$.

DISCUSSION

In McMillan's formalism [34], the electron-phonon coupling strength is given by $\lambda_{\text{ep}} = \left[N(E_F) \langle I^2 \rangle \right] / \left[M \langle \omega^2 \rangle \right]$,

where M stands for the atomic mass, $\langle I^2 \rangle$ and $\langle \omega^2 \rangle$ are averages of the squared electronic matrix elements on the Fermi surface, and of the squared phonon frequencies, respectively. There are thus at least two approaches to enhance

λ_{ep} : one is to increase $N(E_F)$, and the other is to lower $\langle \omega^2 \rangle$ (or, in other words, to soften the lattice). In $\text{Mo}_5\text{Si}_{3-x}\text{P}_x$, $N(E_F)$ is enhanced by electron doping, which shifts E_F to a peak in DOS. The lattice has been effectively softened

too, as evidenced by the large decrease of Θ_D . These two factors together give rise to the strong electron-phonon coupling, and should be responsible for the emergence of superconductivity in $\text{Mo}_5\text{Si}_{3-x}\text{P}_x$. The reason why P doping softens the lattice so much (unlike Re doping in $\text{Mo}_{5-x}\text{Re}_x\text{Si}_3$, which did not change Θ_D much [24]) is definitely worth further studies. Theoretical calculations of the phonon dispersions of $\text{Mo}_5\text{Si}_{3-x}\text{P}_x$ will be illuminating. In particular, large phonon linewidths or soft modes can be expected.

As for the topological properties, although our results suggest that P doping may not be beneficial to the TSSs, there are other ways to chase for topological superconductivity in this system. We notice that the band gap between bands 156 and 158 is topologically nontrivial with strong topological indexes of (1;000) (see Figure 5(f)). Therefore, TSSs are likely to survive and topological superconductivity may be realized, if superconductivity can be induced by hole doping in Mo_5Si_3 . Another strategy is to fabricate $\text{Mo}_5\text{Si}_3/\text{Mo}_5\text{Si}_{1.5}\text{P}_{1.5}$ heterojunctions to see whether TSS emerges from the proximity effect. Given the fact that high-quality Mo_5Si_3 single crystals are readily available [29], $\text{Mo}_5\text{Si}_{3-x}\text{P}_x$ serves as a suitable platform to observe the possibly existing Majorana zero modes, which will be an intriguing topic in future ARPES or STM studies.

Lastly, we should mention that the T_c of 10.8 K and $\mu_0 H_{c2}(0)$ of 14.56 T are fairly high for a pseudobinary compound. For example, both of them are slightly higher than those in the commercial superconductor NbTi ($T_c = 9.6$ K, $\mu_0 H_{c2}(0) = 14$ T) [40]. Most absorbingly, $\text{Mo}_5\text{Si}_{3-x}\text{P}_x$ shares much in common with *A15* superconductors such as V_3Si or Nb_3Sn . For instance, they have similar T_c s, close coupling strength, and all of them show upwards concave features in normal state $\rho(T)$ [30, 41]. Recent theoretical studies suggested nontrivial band topologies in some of the *A15* superconductors too [42]. Compared to the well-known *A15* superconductor family, the W_5Si_3 -type superconductor family, which $\text{Mo}_5\text{Si}_{3-x}\text{P}_x$ belongs to, has not been studied in depth. Currently, the family contains about ten members. Most of them superconduct below 4 K, with the maximal T_c of 5.8 K observed in $\text{Mo}_3\text{Re}_2\text{Si}_3$ [24, 43-48]. Our study almost doubles this maximum, making it comparable with those in the *A15* family. W_5Si_3 -type compounds are hence a fertile ground to be explored for new superconductors.

CONCLUSIONS

To summarize, we discover that P doping introduces superconductivity in non-superconducting Mo_5Si_3 , which hosts a nontrivial band topology. T_c increases with the doping level, reaching 10.8 K in $\text{Mo}_5\text{Si}_{1.5}\text{P}_{1.5}$. $\text{Mo}_5\text{Si}_{1.5}\text{P}_{1.5}$ is a type-II, fully gapped superconductor with strong electron-phonon coupling, as evidenced by the large values of $\Delta C_e/\gamma T_c$, $\Delta_0/k_B T_c$, and λ_{ep} . $\mu_0 H_{c1}(0)$ and $\mu_0 H_{c2}(0)$ for $\text{Mo}_5\text{Si}_{1.5}\text{P}_{1.5}$ are 105 mT and 14.56 T, respectively. According to first-principles calculations, the large electron-phonon coupling is related to the increase of $N(E_F)$. $\text{Mo}_5\text{Si}_{1.5}\text{P}_{1.5}$ sets a new record of T_c in W_5Si_3 -type superconductors. Compared to the previously reported $\text{Mo}_3\text{Re}_2\text{Si}_3$ superconductor [24], or the widely used commercial superconducting material NbTi [40], the higher T_c and inexpensive raw materials of $\text{Mo}_5\text{Si}_{3-x}\text{P}_x$ make future applications promising. We point out that the superconducting properties of $\text{Mo}_5\text{Si}_{3-x}\text{P}_x$ are very similar with those in the *A15* superconductors. Our findings suggest that the T_c levels in W_5Si_3 -type superconductors can be comparable with the *A15* superconductors. Novel superconductors with higher T_c values can be anticipated in W_5Si_3 -type structural family. In particular, superconductivity, or even topological superconductivity, could be achieved through carrier doping, whose effectiveness has been testified in our study.

References

- 1 Kitaev AY. Unpaired Majorana fermions in quantum wires. *Phys-Usp*, 2001, 44: 131
- 2 Qi XL, Zhang SC. Topological insulators and superconductors. *Rev Mod Phys*, 2011, 83: 1057
- 3 Sato M, Ando Y. Topological superconductors: a review. *Rep Prog Phys*, 2017, 80: 076501
- 4 Ivanov DA. Non-abelian statistics of half-quantum vortices in p -wave superconductors. *Phys Rev Lett*, 2001, 86: 268-271
- 5 Lin R, Wang Z. A brief review on Majorana bound states in topological superconductors. *Sci China: Phys, Mech Astron*, 2016, 59: 677401
- 6 Kallin C. Chiral p -wave order in Sr_2RuO_4 . *Rep Prog Phys*, 2012, 75: 042501
- 7 Fu LA, Berg E. Odd-Parity Topological Superconductors: Theory and Application to $\text{Cu}_x\text{Bi}_2\text{Se}_3$. *Phys Rev Lett*, 2010, 105: 097001
- 8 Sasaki S, Ren Z, Taskin AA, *et al.* Odd-parity pairing and topological superconductivity in a strongly spin-orbit coupled semiconductor. *Phys Rev Lett*, 2012, 109: 217004
- 9 Guguchia Z, von Rohr F, Shermadini Z, *et al.* Signatures of the topological $s(+)$ superconducting order parameter in the type-II Weyl semimetal Td-MoTe_2 . *Nat Commun*, 2017, 8: 1082
- 10 Fu L, Kane CL. Superconducting proximity effect and Majorana fermions at the surface of a topological insulator. *Phys Rev Lett*, 2008, 100: 096407
- 11 Xu JP, Wang MX, Liu ZL, *et al.* Experimental Detection of a Majorana Mode in the core of a Magnetic Vortex inside a Topological Insulator-Superconductor $\text{Bi}_2\text{Te}_3/\text{NbSe}_2$ Heterostructure. *Phys Rev Lett*, 2015, 114: 017001
- 12 Wang EY, Ding H, Fedorov AV, *et al.* Fully gapped topological surface states in Bi_2Se_3 films induced by a d -wave high-temperature superconductor. *Nat Phys*, 2013, 9: 620-624
- 13 Rehman MU, Hua CQ, Lu YH. Topology and ferroelectricity in group-V monolayers. *Chin Phys B*, 2020, 29: 057304
- 14 Hor YS, Williams AJ, Checkelsky JG, *et al.* Superconductivity in $\text{Cu}_x\text{Bi}_2\text{Se}_3$ and its Implications for Pairing in the Undoped Topological Insulator. *Phys Rev Lett*, 2010, 104: 057001
- 15 Sasaki S, Kriener M, Segawa K, *et al.* Topological Superconductivity in $\text{Cu}_x\text{Bi}_2\text{Se}_3$. *Phys Rev Lett*, 2011, 107: 217001
- 16 Liu ZH, Yao X, Shao JF, *et al.* Superconductivity with Topological Surface State in $\text{Sr}_x\text{Bi}_2\text{Se}_3$. *J Am Chem Soc*, 2015, 137: 10512-10515
- 17 Asaba T, Lawson BJ, Tinsman C, *et al.* Rotational Symmetry Breaking in a Trigonal Superconductor Nb-doped Bi_2Se_3 . *Phys Rev X*, 2017, 7: 011009
- 18 Fang Y, Pan J, Zhang D, *et al.* Discovery of Superconductivity in 2M-WS_2 with Possible Topological Surface States. *Adv Mater*, 2019, 31: 1901942
- 19 Sharma MM, Rani P, Sang LN, *et al.* Superconductivity Below 2.5K in $\text{Nb}_{0.25}\text{Bi}_2\text{Se}_3$ Topological Insulator Single Crystal. *J Supercond Novel Magn*, 2020, 33: 565-568
- 20 Sakano M, Okawa K, Kanou M, *et al.* Topologically protected surface states in a centrosymmetric superconductor $\beta\text{-PdBi}_2$. *Nat Commun*, 2015, 6: 8595
- 21 Thirupathiah S, Ghosh S, Jha R, *et al.* Unusual Dirac Fermions on the Surface of a Noncentrosymmetric $\alpha\text{-BiPd}$ Superconductor. *Phys Rev Lett*, 2016, 117: 177001
- 22 Zhang P, Yaji K, Hashimoto T, *et al.* Observation of topological superconductivity on the surface of an iron-based superconductor. *Science*, 2018, 360: 182
- 23 Li YW, Zheng HJ, Fang YQ, *et al.* Observation of topological superconductivity in a stoichiometric transition metal dichalcogenide 2M-WS_2 . *Nat Commun*, 2021, 12: 2874
- 24 Wu J, Hua C, Liu B, *et al.* Doping-Induced Superconductivity in the Topological Semimetal Mo_5Si_3 . *Chem Mater*,

2020, 32: 8930-8937

- 25 Toby BH. EXPGUI, a graphical user interface for GSAS. *J Appl Crystallogr*, 2001, 34: 210-213
- 26 Ruan BB, Yang QS, Zhou MH, *et al.* Superconductivity in a new T₂-phase Mo₅GeB₂. *J Alloys Compd*, 2021, 868: 159230
- 27 Giannozzi P, Baroni S, Bonini N, *et al.* QUANTUM ESPRESSO: a modular and open-source software project for quantum simulations of materials. *J Phys: Condens Matter*, 2009, 21: 395502
- 28 Schlipf M, Gygi F. Optimization algorithm for the generation of ONCV pseudopotentials. *Comput Phys Commun*, 2015, 196: 36-44
- 29 Ito K, Hayashi T, Nakamura H. Electrical and thermal properties of single crystalline Mo₅X₃ (X=Si, B, C) and related transition metal 5-3 silicides. *Intermetallics*, 2004, 12: 443-450
- 30 Wiesmann H, Gurvitch M, Lutz H, *et al.* Simple-Model for Characterizing Electrical-Resistivity in A-15 Superconductors. *Phys Rev Lett*, 1977, 38: 782-785
- 31 Yang W, Lou Z, Zhu Q, *et al.* Superconductivity in noncentrosymmetric Mo₃P single crystal. *Supercond Sci Technol*, 2019, 32: 115014
- 32 McGuire MA, Parker DS. Superconductivity at 9 K in Mo₅PB₂ with evidence for multiple gaps. *Phys Rev B*, 2016, 93: 064507
- 33 Allen PB, Dynes RC. Transition-Temperature of Strong-Coupled Superconductors Reanalyzed. *Phys Rev B*, 1975, 12: 905-922
- 34 McMillan WL. Transition Temperature of Strong-Coupled Superconductors. *Phys Rev*, 1968, 167: 331-344
- 35 Carbotte JP. Properties of Boson-Exchange Superconductors. *Rev Mod Phys*, 1990, 62: 1027-1157
- 36 Tinkham M. *Introduction to Superconductivity* (Dover, New York, City, 1996)
- 37 Padamsee H, Neighbor JE, Shiffman CA. Quasiparticle Phenomenology for Thermodynamics of Strong Coupling Superconductors. *J Low Temp Phys*, 1973, 12: 387-411
- 38 Fu L, Kane CL. Topological insulators with inversion symmetry. *Phys Rev B*, 2007, 76: 045302
- 39 Zhang T, Jiang Y, Song Z, *et al.* Catalogue of topological electronic materials. *Nature*, 2019, 566: 475-479
- 40 Hampshire DP. A barrier to increasing the critical current density of bulk untextured polycrystalline superconductors in high magnetic fields. *Physica C*, 1998, 296: 153-166
- 41 Ho KM, Cohen ML, Pickett WE. Maximum Superconducting Transition-Temperatures in A15 Compounds. *Phys Rev Lett*, 1978, 41: 815-818
- 42 Kim M, Wang CZ, Ho KM. Topological states in A15 superconductors. *Phys Rev B*, 2019, 99: 224506
- 43 Wu JF, Liu B, Cui YW, *et al.* Type-II superconductivity in W₅Si₃-type Nb₅Sn₂Al. *Supercond. Sci. Technol.*, 2019, 32: 045010
- 44 Claeson T, Ivarsson J, Rasmussen SE. Superconductivity of Nb₅Ge₃. *J. Appl. Phys.*, 1977, 48: 3998-3999
- 45 Shishido T, Ukei K, Toyota N, *et al.* Flux Growth of a New Ternary Superconducting Crystal Nb₅Sn₂Ga. *J. Cryst. Growth*, 1989, 96: 1-6
- 46 Shishido T, Ye J, Toyota N, *et al.* Growth and Superconductivity of a New Ternary Intermetallic Compound, Ta₅Ga₂Sn. *Jpn J Appl Phys Part 1*, 1989, 28: 1519-1520
- 47 Xie WW, Luo HX, Seibel EM, *et al.* Superconductivity in Hf₅Sb_{3-x}Ru_x: Are Ru and Sb a Critical Charge-Transfer Pair for Superconductivity? *Chem Mater*, 2015, 27: 4511-4514
- 48 Xie WW, Luo HX, Phelan BF, *et al.* Zr₅Sb_{3-x}Ru_x, a new superconductor in the W₅Si₃ structure type. *J Mater Chem C*, 2015, 3: 8235-8240

Acknowledgements The authors acknowledge financial support by the National Key Research and Development of China (Grant Nos. 2018YFA0704200, 2021YFA1401800, 2018YFA0305602, and 2017YFA0302904), the

National Natural Science Foundation of China (Nos. 12074414, 12074002, and 11774402), and the Strategic Priority Research Program of Chinese Academy of Sciences (Grant No. XDB25000000).

Author contributions Sun JN conceived the project; Ruan BB and Sun JN synthesized the samples and did most of the measurements; Chen Y, Gu YD and Yang QS assisted in some of the measurements; Ruan BB carried out the theoretical calculations and wrote the paper with supports from Zhou MH, Ma MW and Zhao K; Chen GF, Shan L and Ren ZA reviewed the original manuscript; Ren ZA supervised the project. All authors contributed to the general discussion.

Conflict of interest The authors declare that they have no conflict of interest.

Supplementary information The relaxed lattice parameters from DFT compared with the experimental ones, comparison of VCA and supercell results, SEM image and elemental mapping of $\text{Mo}_5\text{Si}_{1.5}\text{P}_{1.5}$, and the subtraction of Mo_3P contribution from the raw data.

Table 1 Crystallographic parameters, measured P contents (EDX), and superconducting T_c of $\text{Mo}_5\text{Si}_{3-x}\text{P}_x$ ($0 \leq x \leq 2.0$).

parameter	$x = 0$	$x = 0.5$	$x = 1.0$	$x = 1.2$	$x = 1.3$	$x = 1.5$	$x = 1.6$	$x = 2.0$
measured P content x	0	0.46(5)	0.96(9)	1.14(12)	1.20(13)	1.43(14)	1.49(16)	1.75(18)
a (Å)	9.6444(1)	9.6128(1)	9.5871(1)	9.5627(1)	9.5555(1)	9.5407(1)	9.5332(1)	9.4956(2)
c (Å)	4.9063(1)	4.9200(1)	4.9345(1)	4.9447(1)	4.9492(1)	4.9582(1)	4.9674(1)	4.9856(2)
x_{Si2} ^{a)}	0.1680(2)	0.1657(3)	0.1656(3)	0.1663(3)	0.1662(2)	0.1666(1)	0.1655(4)	0.1650(4)
x_{Mo2}	0.07694(6)	0.07684(8)	0.0767(1)	0.0771(1)	0.0770(1)	0.07630(4)	0.0767(1)	0.0770(1)
y_{Mo2}	0.22356(7)	0.2232(1)	0.2226(1)	0.2221(1)	0.2219(1)	0.22114(5)	0.2218(2)	0.2214(2)
R_p	1.38%	2.10%	2.11%	2.15%	1.96%	0.94%	1.94%	2.07%
R_{wp}	2.32%	2.89%	2.86%	2.92%	2.62%	1.34%	2.52%	2.75%
χ^2	2.48	2.51	2.08	2.24	1.74	1.56	1.76	1.74
Mo_3P weight fraction ^{b)}	0	3.4%	9.9%	9.4%	6.0%	12.3%	20.6%	30.2%
T_c from $\rho(T)$ (K) ^{c)}	—	6.77	8.70	10.09	10.42	10.74	10.74	10.70
T_c from $\chi(T)$ (K)	—	7.01	9.26	10.18	10.40	10.71	10.54	10.71

a) Wyckoff positions: Si1 ($4a$), Si2 ($8h$), Mo1($4b$), Mo2($16k$). P randomly takes the Si1 and Si2 sites. $x_{\text{Si1}} = y_{\text{Si1}} = z_{\text{Si1}} = z_{\text{Si2}} = x_{\text{Mo1}} = z_{\text{Mo2}} = 0$. $y_{\text{Si2}} = x_{\text{Si2}} + 0.5$. $y_{\text{Mo1}} = 2z_{\text{Mo1}} = 0.5$. b) Determined from XRD refinements. c) Determined from the midpoint of superconducting transition in $\rho(T)$.

Table 2 Superconducting parameters of $\text{Mo}_5\text{Si}_{1.5}\text{P}_{1.5}$. The thermodynamic parameters of Mo_5Si_3 and $\text{Mo}_5\text{Si}_2\text{P}$ are also listed for comparison.

parameter	unit	$\text{Mo}_5\text{Si}_{1.5}\text{P}_{1.5}$		
T_c^{onset}	K	10.80		
T_c^{zero}	K	10.70		
$\mu_0 H_{c1}(0)$	mT	105		
$\mu_0 H_{c2}(0)$	T	14.56		
$\mu_0 H_c(0)$	T	0.75		
ζ_{GL}	nm	4.75		
λ_{GL}	nm	70.5		
κ	—	14.8		
parameter	unit	Mo_5Si_3	$\text{Mo}_5\text{Si}_2\text{P}$	$\text{Mo}_5\text{Si}_{1.5}\text{P}_{1.5}$
β	$\text{mJ mol}^{-1} \text{K}^{-4}$	0.054	0.24	0.50
γ	$\text{mJ mol}^{-1} \text{K}^{-2}$	19.80	25.10	37.23
Θ_D	K	659	404	314
λ_{ep}	—	—	0.69 ^{e)}	1.15 ^{d)}
$\Delta C_e/\gamma T_c$	—	—	2.03	2.06
$\Delta_0/k_B T_c$	—	—	2.03	2.14
$N(E_F)$ ^{a)}	$\text{eV}^{-1} \text{f.u.}^{-1}$	—	6.30	7.30
$N'(E_F)$ ^{b)}	$\text{eV}^{-1} \text{f.u.}^{-1}$	4.13	7.24	8.04

a) Experimental value calculated from γ . b) Theoretical value from DFT calculations. c) Estimated from Equation (4). d) Estimated from Equations (1) and (2).

Figure 1 (a) Crystal structure of $\text{Mo}_5\text{Si}_{3-x}\text{P}_x$. (b) XRD patterns of $\text{Mo}_5\text{Si}_{2.5}\text{P}_{0.5}$ and $\text{Mo}_5\text{Si}_{1.5}\text{P}_{1.5}$ with their Rietveld refinements. (c) Evolution of lattice parameters a and c upon P doping. (d) The composition $\text{Mo}_5\text{Si}_m\text{P}_n$ determined from EDX measurements. (e) XRD patterns of $\text{Mo}_5\text{Si}_{3-x}\text{P}_x$ ($0 \leq x \leq 2.0$), with a zoom-in of the (141) peak shown in (f).

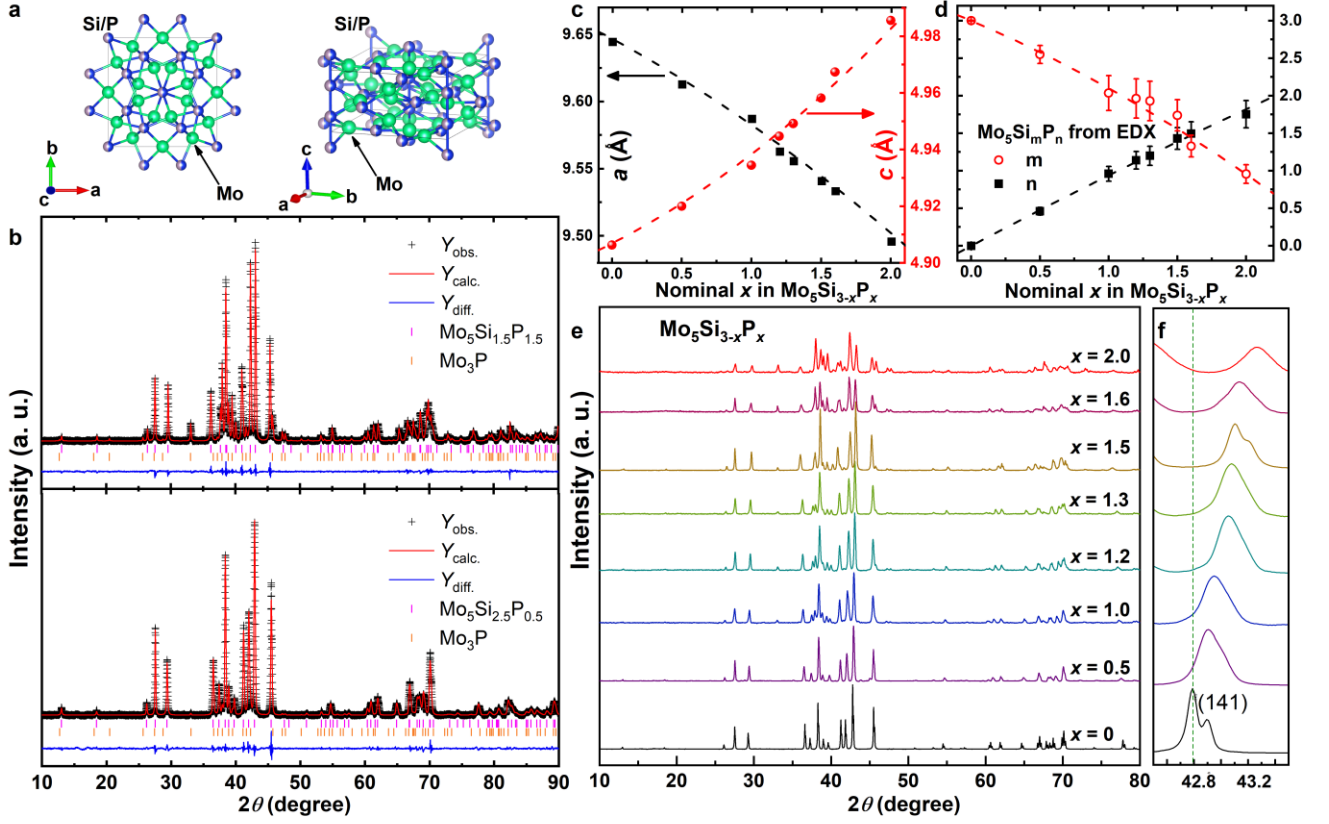


Figure 2 (a) Temperature dependence of resistivity of $\text{Mo}_5\text{Si}_{3-x}\text{P}_x$ ($0 \leq x \leq 2.0$) under zero magnetic field. (b) Zoom-in of the datasets in (a) below 15 K. (c) DC magnetic susceptibility of $\text{Mo}_5\text{Si}_{3-x}\text{P}_x$ ($0 \leq x \leq 2.0$). (d) Evolution of T_c , as well as RRR, with regard to the P doping content x .

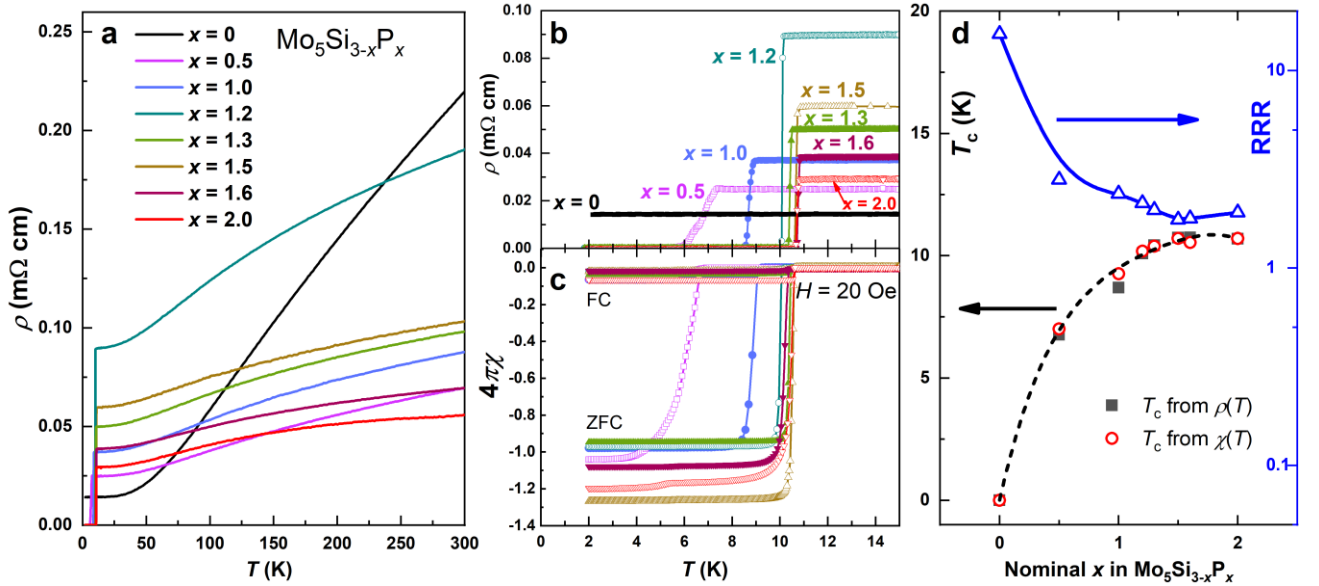


Figure 3 (a) Superconducting transition on $\rho(T)$ of $\text{Mo}_5\text{Si}_{1.5}\text{P}_{1.5}$ under magnetic fields up to 15.5 T. (b) Isothermal magnetization curves of $\text{Mo}_5\text{Si}_{1.5}\text{P}_{1.5}$ at low temperature. (c) Superconducting hysteresis loop of $\text{Mo}_5\text{Si}_{1.5}\text{P}_{1.5}$ at 2 K. (d) Temperature dependence of the upper and lower critical fields of $\text{Mo}_5\text{Si}_{1.5}\text{P}_{1.5}$.

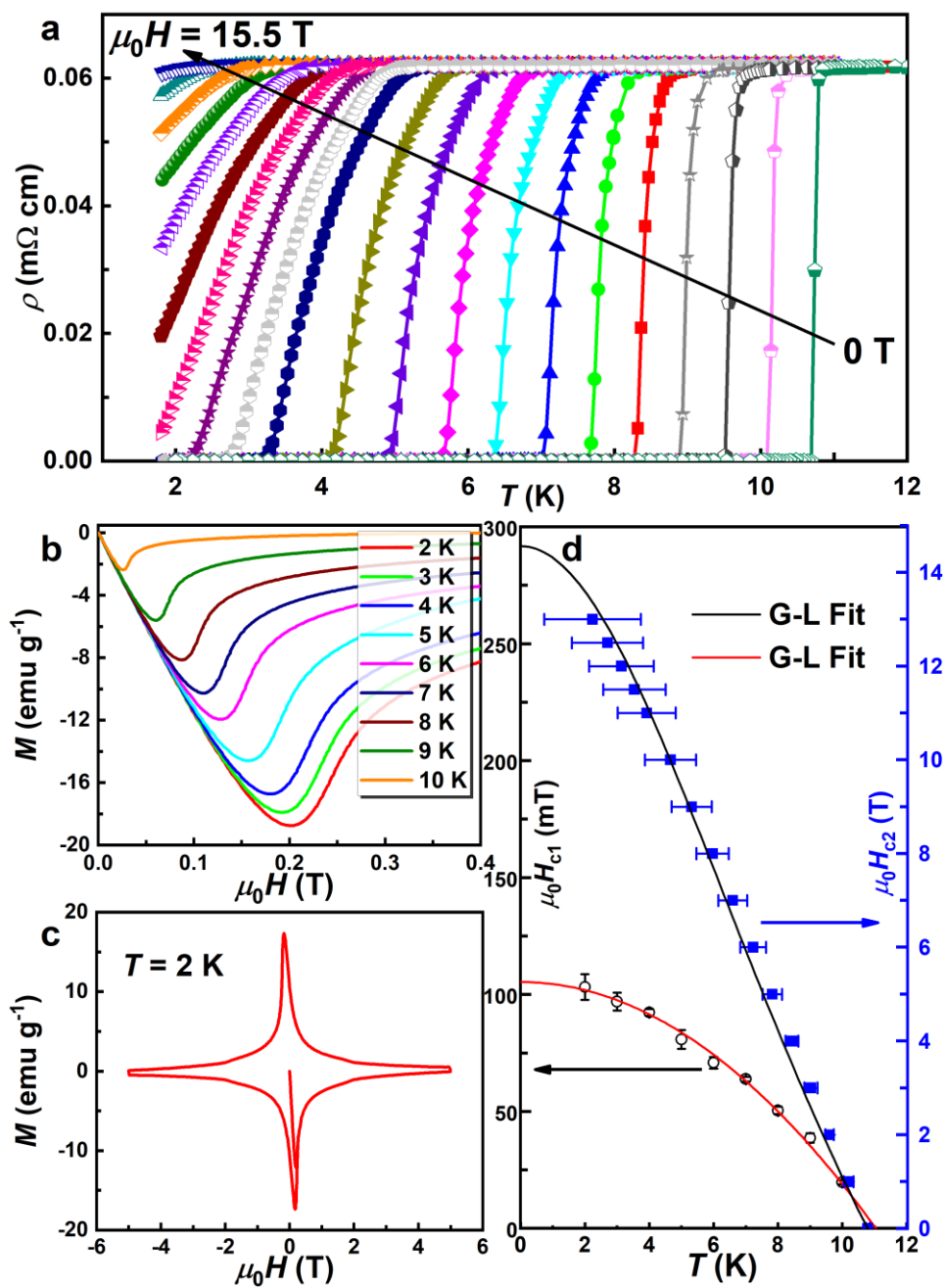


Figure 4 (a) Temperature dependence of heat capacity of $\text{Mo}_5\text{Si}_{3-x}\text{P}_x$ ($x = 0, 1.0, 1.5$) under zero magnetic field. The dash lines are fits to the normal state data with the Debye model. (b) Electronic contribution of heat capacity of $\text{Mo}_5\text{Si}_2\text{P}$ and $\text{Mo}_5\text{Si}_{1.5}\text{P}_{1.5}$. The data below T_c are fitted with the α model, shown as the dash lines. Notice the data for $x = 1.0$ and 1.5 in (a) and (b) have been corrected by subtracting the Mo_3P contributions. The kinks at around 5.6 K are the residual signals from Mo_3P impurity.

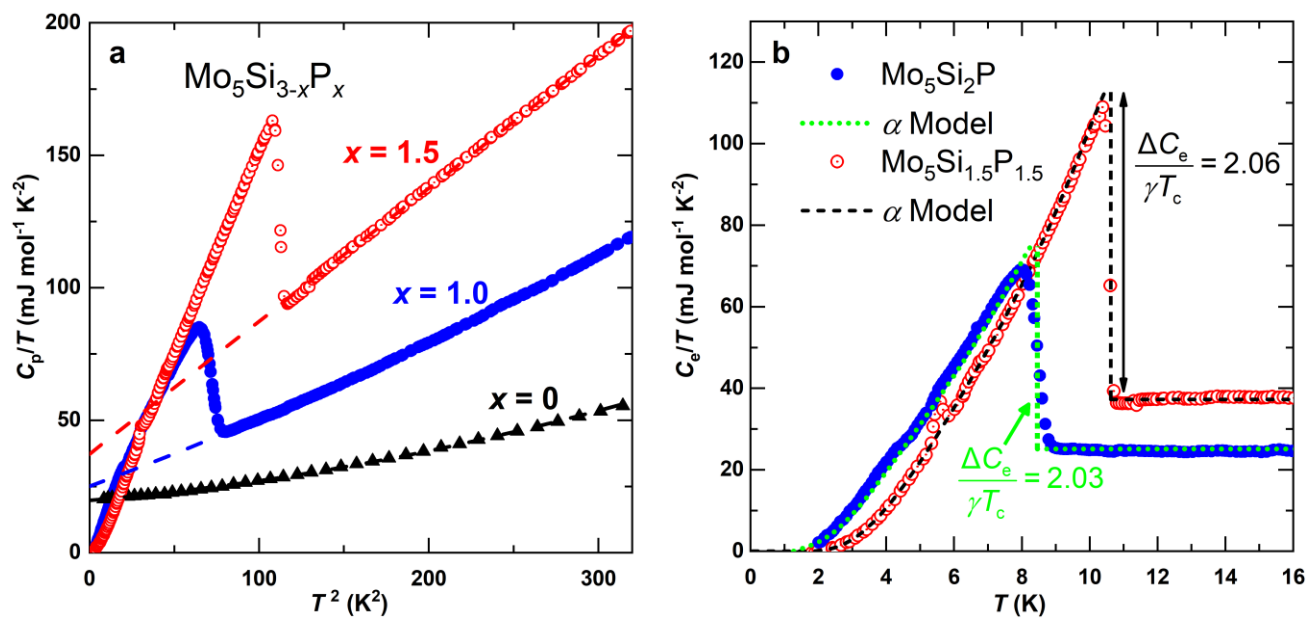


Figure 5 (a) Band structure of Mo_5Si_3 without SOC. (b) Band structure of Mo_5Si_3 with SOC. (c) Band structure of $\text{Mo}_5\text{Si}_2\text{P}$ without SOC. (d) Band structure of $\text{Mo}_5\text{Si}_{1.5}\text{P}_{1.5}$ without SOC. The shadowy boxes in (a)–(d) emphasize the flat band dispersions. (e) Brillouin zone of $\text{Mo}_5\text{Si}_{3-x}\text{P}_x$, with high symmetry points labeled. (f) The Z_2 topological invariants of Mo_5Si_3 (with SOC) for the bands near E_F . The band numbers correspond to those in (b). (g) Evolution of DOS of $\text{Mo}_5\text{Si}_{3-x}\text{P}_x$ ($x = 0, 1.0, 1.5$) upon P doping.

